RESEARCH ARTICLE

AG-221, a First-in-Class Therapy Targeting Acute Myeloid Leukemia Harboring Oncogenic *IDH2* Mutations

Katharine Yen[1], Jeremy Travins[1], Fang Wang[1], Muriel D. David[2,3,4], Erin Artin[1], Kimberly Straley[1], Anil Padyana[1], Stefan Gross[1], Byron DeLaBarre[1], Erica Tobin[1], Yue Chen[1], Raj Nagaraja[1], Sung Choe[1], Lei Jin[1], Zenon Konteatis[1], Giovanni Cianchetta[1], Jeffrey O. Saunders[1], Francesco G. Salituro[1], Cyril Quivoron[2,3,4], Paule Opolon[5], Olivia Bawa[5], Véronique Saada[2,3,4], Angelo Paci[6], Sophie Broutin[6], Olivier A. Bernard[2,3,4], Stéphane de Botton[2,3,4], Benoît S. Marteyn[7,8,9], Monika Pilichowska[10], YingXia Xu[11], Cheng Fang[11], Fan Jiang[12], Wentao Wei[12], Shengfang Jin[1], Lee Silverman[1], Wei Liu[1], Hua Yang[1], Lenny Dang[1], Marion Dorsch[1], Virginie Penard-Lacronique[2,3,4], Scott A. Biller[1], and Shin-San Michael Su[1]

ABSTRACT Somatic gain-of-function mutations in isocitrate dehydrogenases (*IDH*) 1 and 2 are found in multiple hematologic and solid tumors, leading to accumulation of the oncometabolite (*R*)-2-hydroxyglutarate (2HG). 2HG competitively inhibits α-ketoglutarate–dependent dioxygenases, including histone demethylases and methylcytosine dioxygenases of the TET family, causing epigenetic dysregulation and a block in cellular differentiation. *In vitro* studies have provided proof of concept for mutant IDH inhibition as a therapeutic approach. We report the discovery and characterization of AG-221, an orally available, selective, potent inhibitor of the mutant IDH2 enzyme. AG-221 suppressed 2HG production and induced cellular differentiation in primary human *IDH2* mutation–positive acute myeloid leukemia (AML) cells *ex vivo* and in xenograft mouse models. AG-221 also provided a statistically significant survival benefit in an aggressive IDH2^{R140Q}-mutant AML xenograft mouse model. These findings supported initiation of the ongoing clinical trials of AG-221 in patients with *IDH2* mutation–positive advanced hematologic malignancies.

SIGNIFICANCE: Mutations in *IDH1/2* are identified in approximately 20% of patients with AML and contribute to leukemia via a block in hematopoietic cell differentiation. We have shown that the targeted inhibitor AG-221 suppresses the mutant IDH2 enzyme in multiple preclinical models and induces differentiation of malignant blasts, supporting its clinical development. *Cancer Discov; 7(5); 478–93. ©2017 AACR.*

See related commentary by Thomas and Majeti, p. 459.

See related article by Shih et al., p. 494.

INTRODUCTION

Metabolic reprogramming is a hallmark of cancer, contributing to the initiation and maintenance of tumors (1, 2). The NADP$^+$-dependent isocitrate dehydrogenases (IDH) are critical metabolic enzymes that interconvert isocitrate and α-ketoglutarate (αKG). Recurrent somatic point mutations in active site arginine residues of IDH1 (R132) and IDH2 (R140 and R172) have been found in multiple tumors, including acute myeloid leukemia (AML; refs. 3–9). Cancer-associated *IDH1/2* mutations confer the neomorphic activity of reducing αKG to the oncometabolite (*R*)-2-hydroxyglutarate (2HG; refs. 9–11). 2HG accumulation competitively inhibits αKG-dependent dioxygenases, including histone demethylases and methylcytosine dioxygenases of the TET family that regulate cellular epigenetic status (12–15). This epigenetic dysregulation is associated with impairment of cellular differentiation in multiple cell types, including hematopoietic cells (15–21). AGI-6780, a selective sulfonamide inhibitor of the mutant IDH2 enzyme, lowered 2HG levels and induced differentiation of TF-1 erythroleukemia cells and primary human AML cells harboring the *IDH2*^{R140Q} mutation (17), providing *in vitro* evidence that inhibition of the mutant IDH2 enzyme can reverse some of the phenotypic changes it induces. Others have reported similar findings with mutant IDH1 inhibitor tool compounds in AML models (22).

IDH mutations are also found in premalignant disorders, including myelodysplastic syndromes (MDS), and were shown to drive leukemic transformation in cooperation with other genetic events in *IDH*-mutant mouse models of AML (23–25). It is possible that *IDH*-mutant cells drive clonal hematopoiesis, sustaining a reservoir of stem cells associated with resistance to conventional chemotherapy that needs to be targeted via alternative mechanisms (26–28).

Here, we report the design and characterization of AG-221 (enasidenib), an orally available, selective, potent, triazine inhibitor of the mutant IDH2 enzyme that dramatically reduced 2HG levels in multiple models. AG-221 induced differentiation in *IDH2*-mutant TF-1 cells and primary human AML cells *ex vivo*, as well as in four *IDH2*^{R140Q}-mutant human AML xenograft mouse models *in vivo*, and provided a dose-dependent, statistically significant survival benefit *in vivo* in an aggressive human AML xenograft model, supporting its clinical development.

[1]Agios Pharmaceuticals, Inc., Cambridge, Massachusetts. [2]INSERM U1170, Villejuif, France. [3]Gustave Roussy, Université Paris-Saclay, Villejuif, France. [4]Equipe Labellisée Ligue Contre le Cancer, Villejuif, France. [5]Plateforme d'évaluation préclinique, Gustave Roussy, Université Paris-Saclay, Villejuif, France. [6]Service de Pharmacologie, Département de Biologie et Pathologie Médicales, Gustave Roussy, Université Paris-Saclay, Villejuif, France. [7]Unité de Pathogénie Microbienne Moléculaire, Institut Pasteur, Paris, France. [8]INSERM U1202, Institut Pasteur, Paris, France. [9]Laboratoire de Thérapie Cellulaire, Gustave Roussy, Université Paris-Saclay, Villejuif, France. [10]Department of Pathology, Tufts Medical Center, Boston, Massachusetts. [11]ShangPharma, Shanghai, China. [12]Viva Biotech Ltd., Shanghai, China.

Note: Supplementary data for this article are available at Cancer Discovery Online (http://cancerdiscovery.aacrjournals.org/).

K. Yen, J. Travins, F. Wang, and M.D. David contributed equally to this work.

Current address for K. Straley: Vertex Pharmaceuticals, Boston, Massachusetts; current address for B. DeLaBarre: The Consulting Biochemist, LLC, Arlington, Massachusetts; current address for J.O. Saunders: Resilience Therapeutics, Boston, Massachusetts; and current address for F.G. Salituro: SAGE Therapeutics, Cambridge, Massachusetts.

Corresponding Author: Shin-San Michael Su, Agios Pharmaceuticals, Inc., 88 Sidney Street, Cambridge, MA 02139. Phone: 617-649-8600; E-mail: Shinsan.Su@agios.com

doi: 10.1158/2159-8290.CD-16-1034

RESULTS

Discovery of Allosteric Inhibitors of the IDH2-Mutant Enzyme

In pursuit of drug candidates targeting recurrent oncogenic *IDH2* mutations, we initiated a high-throughput screen for inhibitors of the enzyme carrying the most prevalent *IDH2* mutation in AML, *IDH2*^{R140Q} (29–31). Several triazine compounds active against the IDH2^{R140Q} homodimer emerged, and initial hit-to-lead chemistry led to compound 1, the first sub–100 nmol/L inhibitor of IDH2^{R140Q} (Fig. 1A). Although fairly potent in enzymatic and cellular assays, it displayed high lipophilicity, leading to solubility-limited absorption *in vivo*. In addition, its poor *in vitro* liver microsomal stability translated to high clearance *in vivo*. X-ray crystallography revealed binding of a compound 1 molecule to an allosteric site located within the homodimer interface of the IDH2^{R140Q}-mutant enzyme, to which the selective sulfonamide inhibitor AGI-6780 also binds (17). These insights guided optimization of the substituents around the triazine core. Through the addition of mildly polar substituents, such as trifluoromethyl pyridine and 2-methyl-2-propanol, AG-221 (Fig. 1A and Supplementary Fig. S1A) was identified to have excellent potency for 2HG inhibition (Table 1), improved solubility, low clearance (0.83 l/h/kg), and good oral bioavailability (41%) *in vivo* in rats (Supplementary Fig. S1B and Supplementary Table S1).

AG-221 Is a Slow Tight Binder of the IDH2^{R140Q}–Mutant Enzyme

Because IDH2 is homodimeric, and somatic *IDH* mutations found in tumors occur in a single allele, with one wild-type (WT) allele, the mutant enzyme likely exists in cells as a mixture of mutant–WT heterodimers and mutant homodimers. As the heterodimer produces 2HG more efficiently than mutant homodimers (32), it is an important molecular target. We therefore characterized the activity of AG-221 against the heterodimer and mutant and WT homodimers.

AG-221 displayed a long residence time on the IDH2^{R140Q} homodimer, with kinetics consistent with slow-onset tight binding inhibition (Supplementary Fig. S2A and S2B). AG-221 showed noncompetitive inhibition against the IDH2^{R140Q} homodimer for the αKG substrate and uncompetitive inhibition against the IDH2^{R140Q} and IDH2^{WT} homodimers for NADPH and $NADP^+$ cofactors, respectively (Supplementary Fig. S3A–S3C). AG-221 displayed time-dependent, nanomolar potency for inhibiting 2HG production by the IDH2^{R140Q} homodimer (IC_{50} = 0.10 μmol/L at 16 hours), the IDH2$^{R140Q/WT}$ heterodimer (IC_{50} = 0.03 μmol/L), and the IDH2$^{R172K/WT}$ heterodimer (IC_{50} = 0.01 μmol/L), and time-dependent, single-digit micromolar potency for inhibition of the canonical forward (oxidative) reaction in the IDH2^{WT} homodimer (IC_{50} = 1.8 μmol/L at 16 hours; Table 1). Similar potency was observed in the forward direction for the IDH2$^{WT/R140Q}$ and IDH2$^{WT/R172K}$ heterodimers, albeit with lower maximum percentage inhibition (range, 75%–64%). AG-221 displayed selectivity for IDH2-mutant homo- and heterodimers over IDH1^{WT} and IDH1^{R132H}-mutant enzymes (Table 1), a panel of kinases (Supplementary Table 2; ref. 17), and a second panel of 80 receptors, ion channels, and enzymes (data not shown). Furthermore, AG-221 displayed excellent potency in reducing 2HG in cell lines ectopically expressing or overexpressing IDH2^{R140Q} or IDH2^{R172K} (Table 2). In these assays, AG-221 displayed higher potency against R140Q versus R172K; this was not observed in the enzyme assays.

AG-221 Stabilizes the Inhibitory Open Homodimer Conformation of IDH2^{R140Q}

A high-resolution (1.55 Å) X-ray crystal structure of AG-221 in complex with IDH2^{R140Q}, NADPH, and Ca^{2+} (IDH2^{R140Q}.AG-221) confirmed that it binds to the allosteric site enclosed within the homodimer interface, and consequently the mutant enzyme adopts an open conformation. We observed alternative conformations for AG-221 binding in the pocket, owing to the pseudo 2-fold symmetric nature of the pocket (Fig. 1B). To understand the molecular mechanism of inhibition, we crystallized the 1.54 Å resolution X-ray structure of IDH2^{R140Q} bound to substrate αKG, NADPH, and Ca^{2+} (IDH2^{R140Q}.αKG). This catalytically primed complex adopts a compact closed homodimer conformation (Fig. 1C). Comparing the quaternary complexes of IDH2^{R140Q}.AG-221 and IDH2^{R140Q}.αKG suggested that AG-221 allosterically stabilizes the open homodimer conformation, preventing the conformational change required for catalysis, consistent with the mode of inhibition documented for IDH1^{R132H} mutants (17, 33).

AG-221 binding is anchored by multiple hydrogen bonds and hydrophobic interactions within the pocket. The pocket is encapsulated by four helices (α9, α10, α9', α10') lining the sides, two loops (L1 and L1'), and the Y311–D312 interaction pairs capping the ends (Fig. 1D). Nitrogens at the 1, 3 positions on the diaminotriazine core accept hydrogen bonds from the amino sidechain of the Q316 residues, whereas linker amides donate hydrogen bonds to the Q316 carbonyl sidechain (Fig. 1E). The Q316 carbonyl also accepts a hydrogen bond from the 2-methyl-2-propanol moiety of AG-221. Other polar interactions include a halogen bond between AG-221's trifluoromethylpyridine and the D312 capping residue. In addition, van der Waals interactions from surrounding hydrophobic residues W164, V294, V297, L298, V315, I319, and L320 contribute to AG-221's high inhibitory potency. The dominant hydrophobic nature of the pocket reveals why larger polar substituents were less favorable, owing to a steric clash or desolvation energetic penalty. Along with the domain motions, movement of L1 and L1' would be required to provide access to the binding site (17). The collective structural rearrangements needed to access the deeply buried pocket, combined with the multitude of interactions upon binding, explain the slow-on/slow-off tight binding kinetics of AG-221.

AG-221 Inhibited 2HG Production and Induced Differentiation in IDH2-Mutant TF-1 Cells and Primary Human AML Blasts

As reported previously (17), and consistent with observations in myeloblasts from patients with *IDH1/2*-mutant AML (34), IDH2^{R140Q} expression in the TF-1 erythroleukemia cell line induced intracellular 2HG production to concentrations of 3,500 to 5,116 ng/10^6 cells; intracellular and

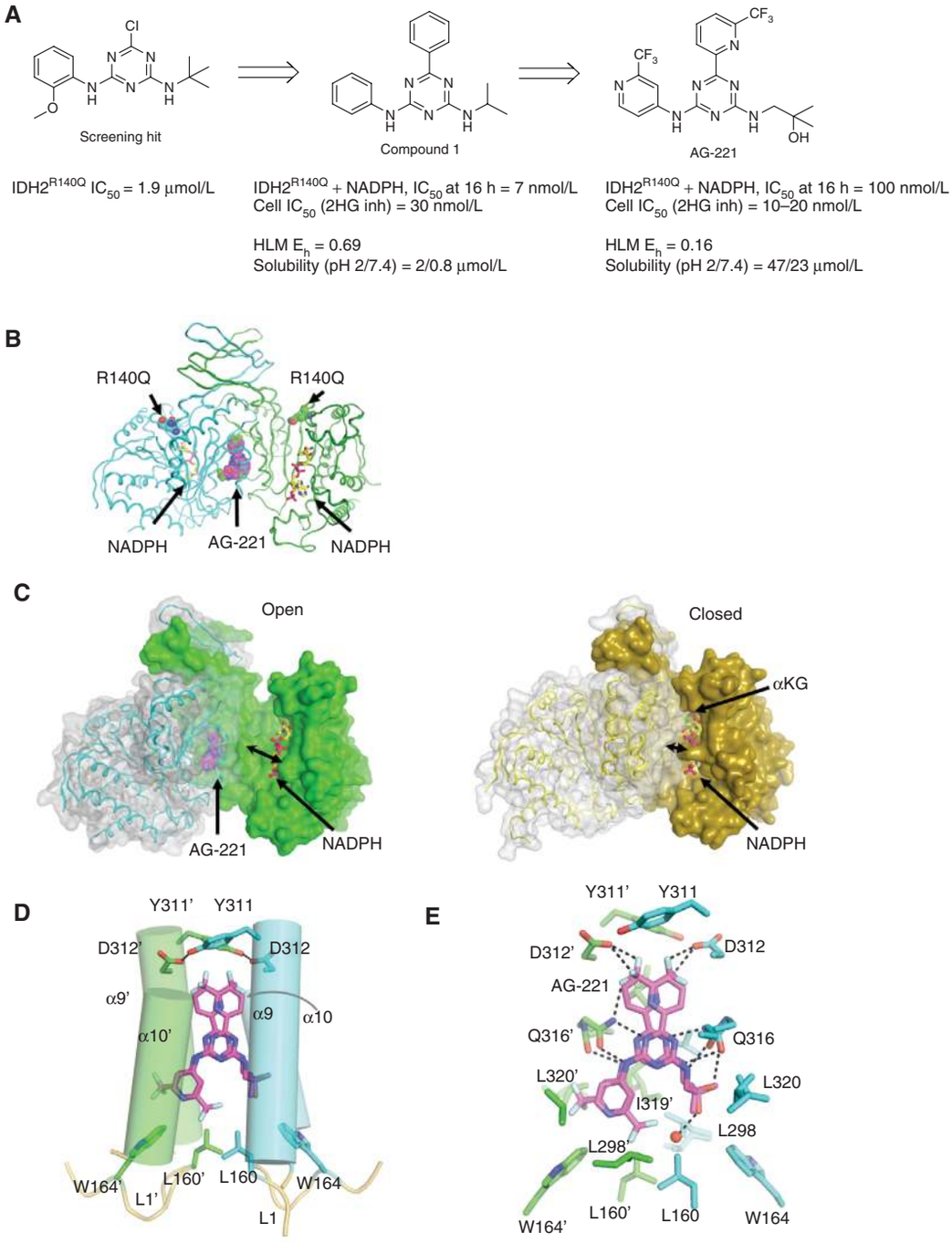

Figure 1. AG-221 structure and binding characteristics. **A,** Key molecules leading to candidate AG-221 and corresponding *in vitro* and biochemical data. **B,** Co-complex crystal structure of $IDH2^{R140Q}$ homodimer with AG-221 bound to an allosteric site. Protein represented as ribbon (protomers colored cyan and green), AG-221 as magenta spheres, and NADPH as yellow sticks. **C,** Allosteric binding of AG-221 stabilizes inhibitory open conformation of the $IDH2^{R140Q}$ active site (left) versus the catalytically primed αKG-bound $IDH2^{R140Q}$ structure (right). Solvent-accessible surface for each protomer shown as translucent white area with cyan or yellow ribbon and solid green or yellow surface for $IDH2^{R140Q}$:AG-221 and $IDH2^{R140Q}$:αKG, respectively. αKG and NADPH shown in ball and stick representation, and AG-221 as solid spheres. **D,** Detailed view of AG-221 binding site at the $IDH2^{R140Q}$ dimer interface. Secondary structures flanking the compound shown as cylinders α9 and α9′ (residues 292–299), and α10 and α10′ (residues 310–325). Residues from each protomer shown in cyan/green. AG-221, shown as sticks (carbon in magenta, nitrogen in blue, fluorines in cyan), exhibits two possible asymmetric binding conformations. Residues Y311 and D312 (stick figures) cap one end of the pocket, and flexible loops L1 and L1′ (residues 151–168; ribbons) cap the other end. **E,** Molecular interactions of AG-221 in its binding site. Amino acid residues within a 3.5 Å radius of AG-221 shown as sticks (green/cyan for carbon atoms from adjacent homodimers). Hydrogen bond interactions between AG-221 and Q316 residue shown as dotted lines. Residues Q316, L320, I319, and V294 exhibit asymmetric alternative conformation in the binding site. E_h, hepatic extraction ratio; HLM, human liver microsome; inh, inhibitory.

Table 1. ***In vitro*** **potency of AG-221 against IDH2-mutant, IDH2^{WT}, and IDH1^{WT} enzymes**

Enzyme	IC_{50} (μmol/L)[a] mean ± SD (max % inh) forward (oxidative)	IC_{50} (μmol/L)[a] mean ± SD (max % inh) reverse (reductive)
IDH2		
IDH2^{R140Q} homodimer + NADPH @ 1 h		0.32 ± 0.05 (99 ± 2)
IDH2^{R140Q} homodimer + NADPH @ 16 h		0.10 ± 0.03 (110 ± 4)
IDH2^{R172K} homodimer + NADPH @ 1 h		0.20 ± 0.07 (86 ± 5)
IDH2^{R172K} homodimer + NADPH @ 16 h		0.40 ± 0.14 (89 ± 5)
IDH2^{WT} homodimer + $NADP^+$ @ 1 h	39.83 ± 9.08[b]	
IDH2^{WT} homodimer + $NADP^+$ @ 16 h	1.80 ± 0.32 (88 ± 2)	
IDH2$^{WT/R140Q}$ heterodimer + $NADP^+$/NADPH @ 1 h	0.38 ± 0.19 (73 ± 2)	0.31 ± 0.17 (96 ± 4)
IDH2$^{WT/R140Q}$ heterodimer + $NADP^+$/NADPH @ 16 h	0.04 ± 0.02 (75 ± 2)	0.03 ± 0.02 (89 ± 8)
IDH2$^{WT/R172K}$ heterodimer + $NADP^+$/NADPH @ 1 h	0.18 ± 0.09 (71 ± 0)	0.11 ± 0.01 (107 ± 4)
IDH2$^{WT/R172K}$ heterodimer + $NADP^+$/NADPH @ 16 h	0.03 ± 0.02 (64 ± 3)	0.01 ± 0.01 (100 ± 2)
IDH1		
IDH1^{WT} homodimer + $NADP^+$ @ 1 h	1.12 ± 0.68 (77 ± 2)	
IDH1^{WT} homodimer + $NADP^+$ @ 16 h	0.45 ± 0.31 (75 ± 1)	
IDH1^{R132H} homodimer + NADPH @ 1 h		77.64 ± 11.99[b]
IDH1^{R132H} homodimer + NADPH @ 16 h		48.40 ± 10.20[b]

NOTE: For activity against enzyme, the enzyme, cofactor, and compound were preincubated for 1 or 16 hours as described in Methods. For all enzyme assessments, $n \geq 3$. The forward (oxidative) reaction refers to conversion of isocitrate and $NADP^+$ to αKG and NADPH, and the reverse (reductive) reaction to conversion of αKG and NADPH to 2HG and $NADP^+$.

Abbreviations: h, hour; inh, inhibitory; max, maximum.

[a]Consistent with the mechanism of action, IC_{50} measurements were carried out in the presence of $NADP^+$ cofactor for the IDH1^{WT} and IDH2^{WT} homodimers; NADPH for the IDH2^{R140Q}, IDH2^{R172K}, and IDH1^{R132H} homodimers; and a mixture of $NADP^+$/NADPH cofactors for the IDH2$^{WT/R140Q}$ and IDH2$^{WT/R172K}$ heterodimers.

[b]Fit to 100% (assay does not reach 100% inhibition at 100 μmol/L maximum compound concentration).

extracellular 2HG levels were reduced by AG-221 treatment (Supplementary Fig. S4A and S4B). AG-221 also inhibited growth factor–independent proliferation and reversed histone H3 hypermethylation induced by IDH2^{R140Q} expression (Supplementary Fig. S4C and S4D).

Treatment of TF-1 cells with erythropoietin (EPO) induces expression of the genes hemoglobin alpha 1 and 2 (*HBA1/2*) and erythroid Kruppel-like factor 1 (*KLF1*), a master regulator of erythropoiesis, and a red color change associated with differentiation. Such EPO-induced changes were not observed in TF-1 cells expressing IDH2^{R140Q} with elevated intracellular 2HG (3,500 ng/10^6 cells; Supplementary Fig. S5A), confirming that this mutation blocks EPO-induced differentiation (17). On AG-221 treatment, dose-dependent increases in *KLF1* and *HBA1/2* expression were seen in IDH2^{R140Q} cells, along with the color change indicative of cellular differentiation (Supplementary Fig. S5A–S5C). Treatment of IDH2^{R140Q}-mutant TF-1 cells with AG-221 did not induce apoptosis, as shown

Table 2. ***In vitro*** **potency of AG-221 for 2HG suppression**

Cell line	Cell origin	Mutation	*n*	IC_{50} (μmol/L) Mean ± SD (max % inh)
HCT-116 KI[a]	Human colorectal carcinoma	IDH2^{R172K}	9	0.53 ± 0.26 (84)
TF-1 pLVX[b]	Human erythroleukemia	IDH2^{R140Q}	3	0.02 ± 0.01 (85)
TF-1 pLVX[b]	Human erythroleukemia	IDH2^{R172K}	3	0.98 ± 0.18 (80)
U87MG pLVX[b]	Human glioblastoma	IDH2^{R172K}	5	1.59 ± 0.42 (58)
U87MG pLVX[b]	Human glioblastoma	IDH2^{R140Q}	9	0.01 ± 0.00 (96)

NOTE: Potency of AG-221 for 2HG suppression in cell lines with endogenous or ectopically expressed IDH2^{R140Q} or IDH2^{R172K} mutations was assessed based on 2HG levels in culture medium. Values are normalized to IDH2-mutant samples treated with DMSO (control).

Abbreviations: inh, inhibitory; max, maximum.

[a]Ectopic expression (knock-in mutation).

[b]Overexpression.

using fluorescence-activated cell sorting (FACS) for propidium iodide/Annexin V staining and cleaved caspase-3 or cleaved PARP protein expression (Supplementary Fig. S5D and S5E).

AG-221 also induced dose-dependent decreases in intracellular 2HG and cellular differentiation in *ex vivo* FACS-sorted primary blasts from patients with IDH2^{R140Q}- or IDH2^{R172K}-mutant AML. Consistent with the IC_{50} values estimated in cell lines (Table 2), primary AML samples expressing IDH2^{R140Q} were more sensitive to the inhibitory action of AG-221 than those harboring the IDH2^{R172K} mutation. When cultured in the presence of 0.1 μmol/L AG-221, IDH2^{R140Q} cells showed an approximately 50% decrease in intracellular 2HG, whereas levels remained high in IDH2^{R172K} cells (Fig. 2A). Consistent results were obtained when levels of 2HG in cell supernatant were considered. AG-221 treatment resulted in an increase in the percentage of cells expressing cell surface markers associated with granulocytic differentiation for both mutations, which was supported by cytology (Fig. 2B and C). Due to the heterogeneity of AML samples, several differentiation markers at several time points should be monitored in order to appreciate the responsiveness of *IDH2*-mutant cells to such inhibitors. Quantitative SNP assay PCR showed conservation of *IDH2* mutant allele frequency following treatment in FACS-sorted mature myeloid cells (Fig. 2D), confirming that these mature cells were derived from IDH2-mutant blasts. We next evaluated the ability of AG-221 to promote the production of mature, functional neutrophils from IDH2-mutant blasts. Following culture in the presence of 5 μmol/L AG-221 for 8 days, IDH2^{R140Q} blast cells (AML-8) exhibited granules colocalizing with lactoferrin (Fig. 2E), a canonical marker of secondary and tertiary granules (35), and a significantly higher number of cells with multilobed nuclei compared with control (mean ± SEM 32.4% ± 3.3% vs. 10.6% ± 1.8%; $P < 0.001$ by Student *t* test; Fig. 2F). Enhanced phagocytosis of opsonized latex beads was observed in AG-221–treated cultures on day 8 of treatment compared with control (mean ± SEM 66.5% ± 2.9% vs. 25.3% ± 9.3%; $P < 0.001$ by Student *t* test), illustrating the functional integrity of IDH2^{R140Q} neutrophils (Fig. 2E and F). These data evidence a reprogramming of granulopoiesis upon AG-221 treatment, resulting in fully mature and functional neutrophils.

Together, these data indicate inhibition of 2HG production and reversal of downstream differentiation effects of the *IDH2*^{R140Q} and *IDH2*^{R172K} mutations.

AG-221 Suppressed Production of 2HG in Tumor Xenograft Models

To investigate the pharmacokinetic and pharmacodynamic effects of AG-221 on the extent and timing of 2HG suppression, we utilized a U87MG IDH2^{R140Q}-mutant subcutaneous mouse xenograft model that exhibits high plasma and intratumoral 2HG concentrations (2,616 ± 86 ng/mL and 2.0 ± 0.10 × 10^6 ng/g, respectively). AG-221 was administered to tumor-bearing mice as a single oral dose (25 or 50 mg/kg), and plasma and tumor concentrations of AG-221 and 2HG, respectively, were monitored over 3 days. AG-221 was detected throughout the study period, displaying rapid absorption and dose-proportional pharmacokinetics between 25 and 50 mg/kg, with a terminal half-life of 6 to 7 hours (Supplementary Fig. S6). 2HG reductions were observed 3 hours after dosing, with maximum reductions 12 hours after dosing of 93.3% and 96.2% in plasma (data not shown), and of 96.6% and 97.1% in tumors at 25 and 50 mg/kg, respectively (Supplementary Fig. S6). In response to decreasing plasma concentrations of AG-221, 2HG levels recovered with time, returning to predose levels 72 hours after dosing, when AG-221 plasma concentrations were < 5 ng/mL. 2HG reduction was even greater after 2 doses of 25 mg/kg given 12 hours apart (99.2% inhibition in tumors 8 hours after second dose), reaching levels observed in the plasma of WT mice (~200 ng/mL).

AG-221 in Primary Human AML Xenograft Models

To explore *in vivo* differentiation effects of AG-221, we established three xenograft models (AML-1, AML-2, AML-3) using freshly isolated, unsorted AML mononuclear cells from patients with IDH2^{R140Q}-mutant AML (Supplementary Table S3). From each model, 10 mice with sustained human CD45-positive (hCD45$^+$) cell counts (range, 16%–66%) in bone marrow (BM) were randomly allocated to vehicle ($n = 5$) or AG-221 30 mg/kg twice daily (BID; $n = 5$) for 38 days.

The treatment was well tolerated: There were no abnormalities in body weight, hematocrit, platelet counts, behavior, or food consumption in either group (Supplementary Fig. S7 and data not shown). Analyses of peripheral blood (PB) samples at multiple time points showed constant AG-221 serum concentration and near-normal 2HG levels in AG-221–treated animals (Supplementary Tables S4 and S5A), indicating effective inhibition of the IDH2^{R140Q}-mutant enzyme. Intracellular 2HG levels also were reduced to below the limit of quantification in BM and spleen on day 38 of AG-221 treatment (Supplementary Table S5B). Upon AG-221 treatment, the hCD45$^+$ subset of PB cells in models AML-1 and AML-2 acquired surface expression of several differentiation markers, including CD11b, CD14, CD15, and CD24 (Fig. 3A). The appearance of differentiated cells was observed between days 10 and 20 and reached >60% of the total human cell number by day 38.

In vehicle-treated mice, hCD45$^+$ immunostaining at time of sacrifice (day 38) revealed large infiltrates of tightly packed positive cells in the BM and spleen, establishing that the human AML cells had homed to hematopoietic organs; these cells had also disseminated to nonhematopoietic tissues such as the liver, kidney, lung, and heart (Fig. 3B, Supplementary Fig. S8A, and data not shown). Hematoxylin–eosin–safranin (HES) staining showed a homogeneous population of immature cells, characterized by large hyperchromatic nuclei with detectable nucleoli (Supplementary Fig. S8B). In AG-221–treated mice, immunostaining on treatment day 38 revealed a dramatic decrease in hCD45$^+$ cells in the BM (for models AML-1, AML-2, and AML-3 combined, mean ± SEM reduction of 71% ± 29%), spleen (reduction 50% ± 12%), and nonhematopoietic organs, and HES staining of the corresponding tissues displayed residual human cells with heterogeneous irregular shape and occasional pyknotic nuclei (Fig. 3B, Supplementary Fig. S8A and S8B, and data not shown). Accordingly, flow cytometry of BM-derived hCD45$^+$ cells showed that AG-221 treatment induced an increase in cell granularity [indicated by an increase in side scatter (SSC)], the acquisition of CD14 or CD15 differentiation markers, and a decrease in

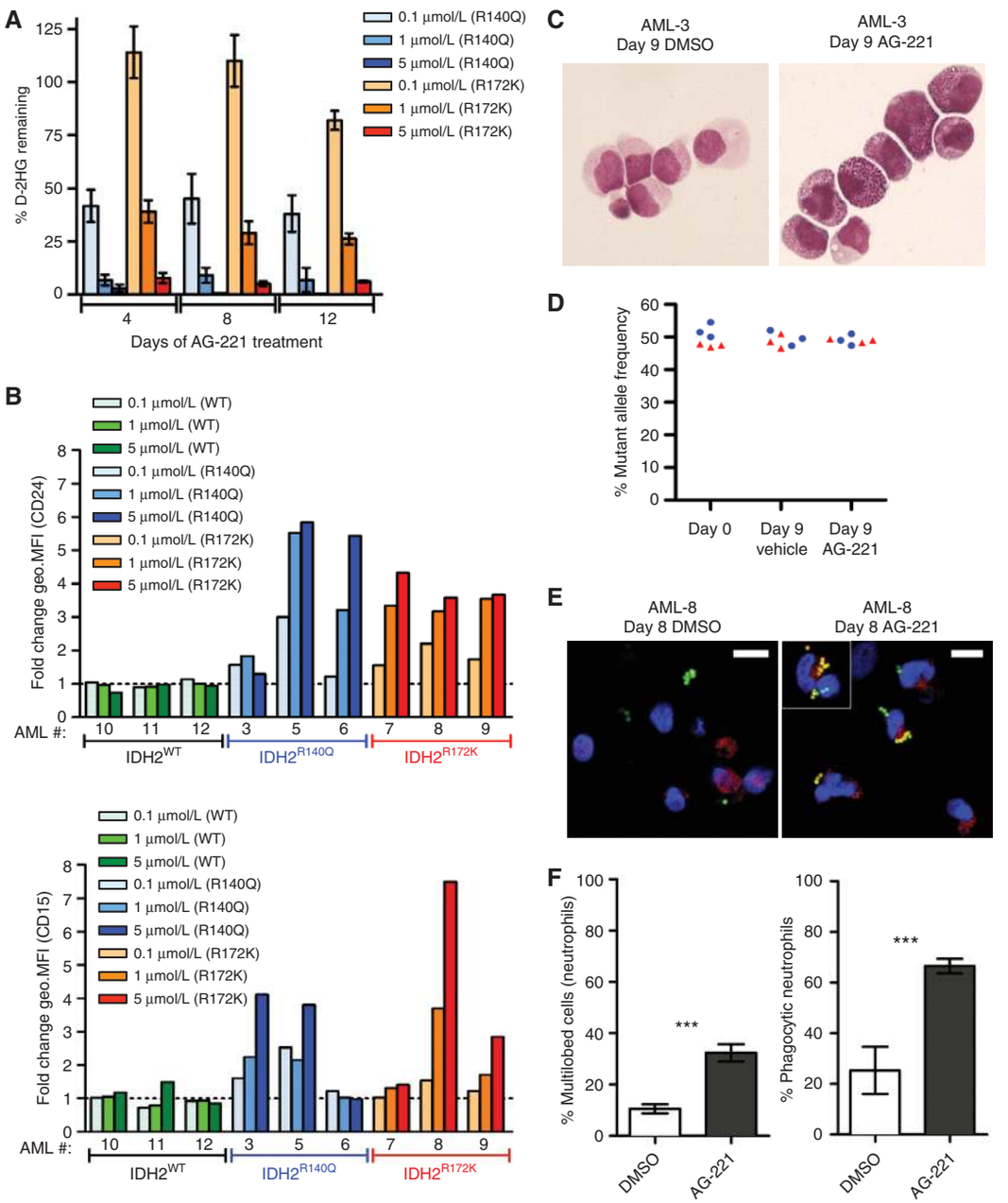

Figure 2. AG-221 can reduce intracellular 2HG levels and induce differentiation in primary human IDH2^{R140Q}- or IDH2^{R172K}-mutant AML patient samples treated *ex vivo*. Cells were cultured in the presence of AG-221 (0.1, 1, or 5 µmol/L) or DMSO (0.1%, v/v, used as a vehicle control) for up to 12 days. **A,** Percentage of intracellular 2HG remaining after 4, 8, and 12 days of treatment with AG-221 relative to DMSO control at the indicated doses. Data are represented as mean ± SEM of the % 2HG remaining ($n = 3$ for each dose per genotype at days 4, 8, and 12). **B,** AG-221–induced fold changes in geometric mean fluorescence intensity (geo.MFI) for the CD24 or CD15 markers at day 8. $P < 0.05$ for 1 µmol/L and $P < 0.01$ for 5 µmol/L AG-221 for both genotypes versus WT by one-way ANOVA followed by Bonferroni corrected comparisons for selected pairs of means (WT vs. R140Q or WT vs. R172K). **C,** Cytology analysis of May-Grünwald-Giemsa–stained BM-derived IDH2^{R140Q}-mutant cells (AML-3) showing granulocytic maturation on day 9 following treatment with 1 µmol/L AG-221 that was not seen in vehicle-treated cells (DMSO). **D,** *IDH2*^{R140Q}- and *IDH2*^{R172K}-mutant allele frequency determined by quantitative SNP assay PCR using DNA from primary AML samples before culture (day 0) and at day 9 following treatment with vehicle or 1 µmol/L AG-221. For the AG-221–treated cell population at day 9, differentiated cells were sorted by FACS according to expression of the CD24, CD15, and/or CD11b differentiation markers. Blue circles show allele frequency in *IDH2*^{R140Q} AML samples ($n = 3$), and red triangles show allele frequency in *IDH2*^{R172K} AML samples ($n = 3$). Results show that allele frequencies were all at approximately 50% in AML blasts carrying *IDH2*^{R140Q} and *IDH2*^{R172K} mutations in all of the indicated conditions. **E,** Confocal microscope images of primary AML cells treated with 5 µmol/L AG-221 (day 8), showing the presence of mature, functional neutrophils. Cells were stained for human lactoferrin (red), and DNA was labeled with DAPI (blue). Neutrophils were identified on the basis of morphologic characteristics (bilobed or multilobed nuclei). Phagocytic activity was assessed using opsonized latex beads (green). Data obtained from AML-8 are shown. Scale bars, 10 µm. **F,** Mature neutrophils (cells with multilobed nuclei), and neutrophils with phagocytic activity (cells with at least one latex bead phagocytized), were quantified in the AG-221– or control (DMSO)-treated cell populations. Data from AML-8 are shown as mean ± SEM. ***, $P < 0.001$ (Student *t* test).

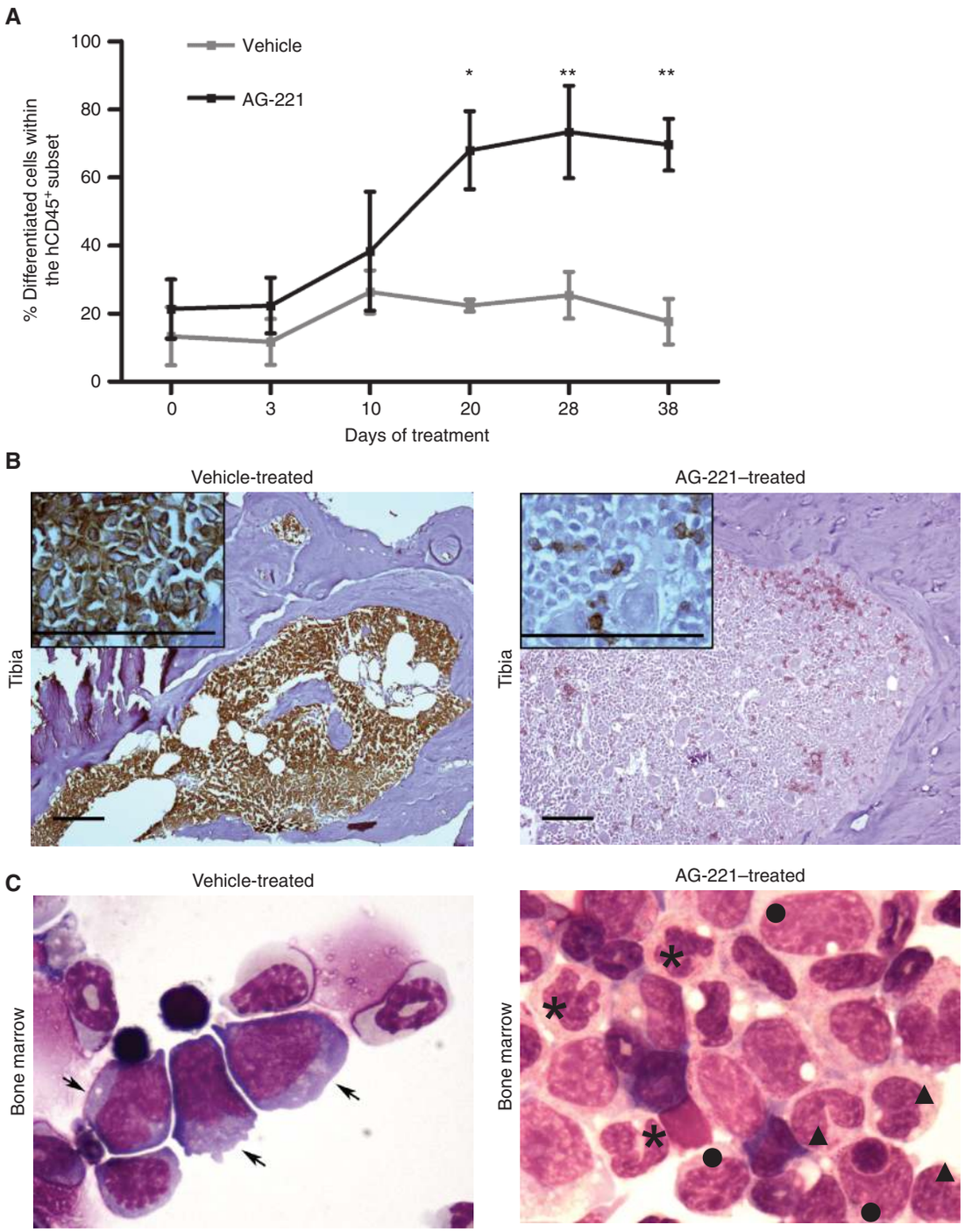

Figure 3. AG-221 induces the differentiation of IDH2R^{140Q} blasts along myeloid lineages in primary human AML xenograft models. **A,** Percentage of hCD45$^+$ cells in the blood expressing any of the cell surface markers associated with differentiation along the monocytic/macrophage and granulocytic lineages (CD11b, CD14, CD15, or CD24) following treatment with AG-221 30 mg/kg b.i.d. or vehicle for 38 days, starting on day 0 (mean ± SD of combined data obtained from AML-1 and AML-2 is shown, $n = 3$ for both vehicle and AG-221). Statistical significance of AG-221–induced differentiation was determined using a two-way ANOVA with Bonferroni post-test corrections. *, $P < 0.005$ and **, $P < 0.001$. The AML-3 model was not included because it displayed very low levels of human cells in the blood; therefore, the effects of AG-221 on this parameter could not be assessed. **B,** hCD45 immunostaining (x100). In AG-221–treated mice, immunostaining revealed a dramatic decrease in hCD45$^+$ cells in the BM (tibia). Representative samples from AML-2 shown. Scale bars, 100 μm. **C,** Cytology analysis of May-Grünwald-Giemsa–stained BM-derived cells illustrates the maturation of human blasts upon treatment with AG-221, as revealed by a decrease in the number of immature cells [blasts displaying cytoplasmic basophilia and high nucleocytoplasmic ratio (indicated by arrows on left plot)] accompanied by an increase in the number of more mature cell types such as myelocytes (black circles, right plot), metamyelocytes (black triangles, right plot), or neutrophils (black stars, right plot). Representative samples from AML-3 shown.

cells expressing the immaturity marker hCD117/c-KIT (Supplementary Fig. S9A and S9B). Cytologic analysis of BM-derived cells on treatment day 38 confirmed a 2- to 35-fold decrease in the percentage of human blasts upon AG-221 treatment, accompanied by an increase in the percentage of mature myeloid cells (Fig. 3C). Analyses of hCD45$^+$ cells from the spleen also revealed AG-221–induced cell differentiation. Finally, the percentage of differentiated cells in the hCD45$^+$ cell population in the BM was higher in AG-221–treated versus vehicle-treated mice, and quantitative SNP assay PCR confirmed the presence of the *IDH2*^{R140Q} mutation (Supplementary Fig. S9C), demonstrating that AML blast cells, rather than cotransplanted normal human hematopoietic cells, had given rise to differentiated cells after *in vivo* AG-221 treatment, which supports a differentiation rather than a cytotoxic effect. These data show that AG-221 can dramatically reduce 2HG in the serum and BM, and reverse the IDH2^{R140Q}-induced differentiation block in primary human AML xenograft models.

AG-221 Conferred a Dose-Dependent Survival Advantage in an Aggressive Human AML Xenograft Mouse Model

To determine if the *in vivo* differentiation effects of AG-221 were associated with a survival benefit, we established an aggressive human xenograft mouse model using early passage cells from a patient with AML harboring IDH2^{R140Q} (AML-4; Supplementary Table S3). Once PB engraftment of hCD45$^+$ AML cells reached approximately 10% (day 48 post–tail vein injection), animals were randomly allocated to vehicle or AG-221 at 5, 15, or 45 mg/kg once daily until end of treatment (day 84) or arabinofuranosyl cytidine (Ara-C) 2 mg/kg once daily for 5 days (Fig. 4A). AG-221 treatment was well tolerated and, compared with vehicle, conferred a dose-dependent survival advantage that was statistically significant at doses of 15 and 45 mg/kg; there was also a statistically significant survival advantage with AG-221 45 mg/kg versus low-dose Ara-C 2 mg/kg given for 5 days ($P < 0.0001$; Fig. 4B). Four animals in the AG-221 45 mg/kg group remained on treatment after day 84, and all survived until study termination (day 130).

This survival advantage was accompanied by reductions in 2HG levels and cell differentiation. As measured 8 hours after last dose (day 84), AG-221 exhibited a linear pharmacokinetic profile and effective inhibition of 2HG production in blood (89.7%, 91.9%, and 93.6%) and spleen (97.8%, 99.8, and 99.9%) at doses of 5, 15, and 45 mg/kg b.i.d., respectively. In BM, 2HG levels were below the limit of quantitation in all AG-221–treated animals except for two in the lowest dose group (both 93.3% inhibition; Supplementary Table S6). On day 84, there was a dose-dependent decrease in the percentage of BM blast cells that was not seen in controls or mice treated with Ara-C for 5 days (Fig. 4C). Similar to the three less aggressive xenograft models (Supplementary Fig. S9C), the *IDH2*^{R140Q} allele frequency in BM samples at termination was in the range of 37% to 52% across different AG-221 doses. Cytology showed the appearance of more mature differentiated myeloid cell forms compared with vehicle-treated mice, characterized by nuclear lateralization, coarse chromatin, and eosinophilic cytoplasm, in contrast to the decrease in cell size and nuclear fragmentation observed with Ara-C (Fig. 4D). Finally, there was a dose-dependent increase in expression of CD15, a granulocytic marker of differentiation, in PB and BM of AG-221–treated mice that was not seen with Ara-C or vehicle (Fig. 5A and B). The lower percentage of differentiated cells seen in this model versus the less aggressive models likely reflects assessment here of only CD15$^+$ cells within the CD45$^+$ subset (additional differentiation markers were assessed in the other models). Interestingly, mice that died of leukemic disease in the 5 and 15 mg/kg dose groups (circled, Fig. 5A and B) failed to express CD15$^+$, suggesting that onset of differentiation may be key to the survival of animals treated with AG-221.

DISCUSSION

There are limitations with currently approved chemotherapies for the treatment of AML, and although standard cytotoxic induction therapy is often effective initially, most patients relapse and become refractory, resulting in poor prognosis (36). *IDH1/2* mutations can be identified in approximately 20% of patients with AML and approximately 5% of patients with MDS (37, 38), and can contribute to leukemia via a block in hematopoietic cell differentiation (16, 17, 23, 24, 39). We have discovered AG-221, an oral, selective, first-in-class inhibitor of the mutant IDH2 enzyme. AG-221 binds to an allosteric site within the dimer interface, stabilizing the open conformation of the enzyme and inhibiting the conversion of αKG to 2HG. AG-221 demonstrates excellent pharmaceutical properties, including adequate solubility, low clearance, and good oral bioavailability, and potently inhibits 2HG production by both the IDH2$^{R140Q/WT}$ heterodimer and IDH2^{R140Q} homodimer. AG-221 shows noncompetitive inhibition with respect to the αKG substrate and uncompetitive inhibition with respect to the NADPH cofactor, and is a slow-on/slow-off inhibitor of the enzyme.

AG-221 exhibited robust 2HG suppression in multiple preclinical *in vitro* and *in vivo* IDH2^{R140Q}-mutant systems, including primary human AML patient cells and xenograft mouse models of primary human AML, supporting its clinical development. In all models, 2HG suppression resulted in a release of the IDH2^{R140Q}-induced cellular differentiation block, which in an aggressive AML xenograft mouse model was associated with a dose-dependent survival advantage versus vehicle that was statistically significant at higher doses. Survival was significantly better in the AG-221 45 mg/kg group compared with the 5-day, low-dose Ara-C group ($P < 0.0001$). Furthermore, with continuous AG-221 treatment, there was a dose-dependent decrease in the number of immature blasts observed in BM and an increase in the number of cells expressing differentiation markers in the BM and PB, supporting a differentiation effect. This was not seen in mice treated with Ara-C (2 mg/kg for 5 days) or in controls. Data showing that the *IDH2*-mutant allele frequency does not change upon AG-221 treatment indicate that mature cells were derived from *IDH2*-mutant blasts and support a differentiation effect. Although terminally differentiated myeloid cells undergo apoptosis, we hypothesize that, because the differentiation effect of AG-221 is slow relative to cytotoxic therapy, the percentage of terminally differentiated cells undergoing apoptosis at any given time point is low, and such cells would not be readily detectable. Our data from the

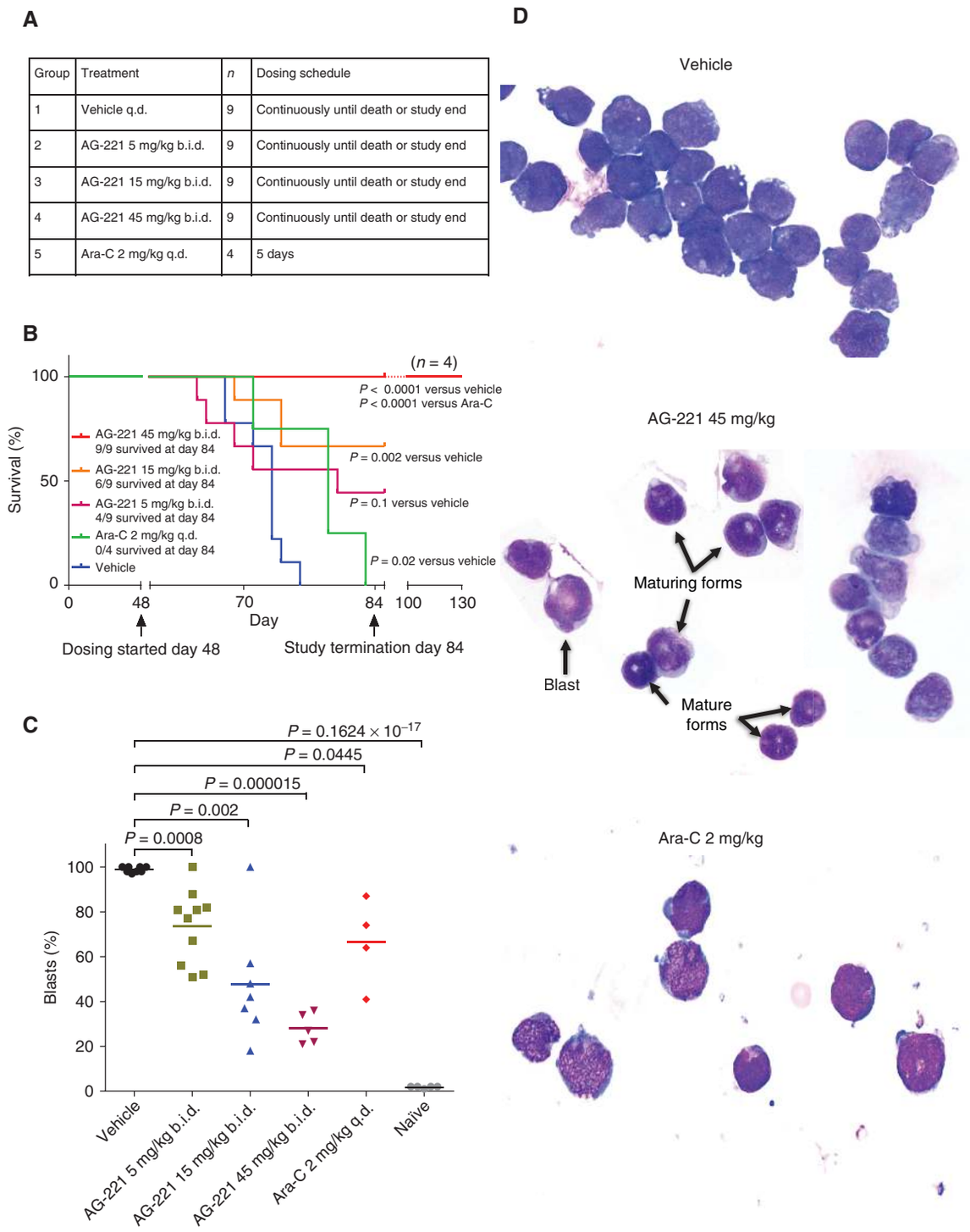

Figure 4. Effects of AG-221 treatment on survival and cell differentiation in an IDH2^{R140Q} primary human AML xenograft model. **A,** Study design outlining random allocation of mice into dosing groups. **B,** Kaplan–Meier survival curves in mice treated with vehicle, AG-221, or low dose Ara-C. Dosing was initiated when tumor burden was approximately 10% in PB/60% in BM (day 48). At day 84, surviving mice were terminated except for four animals in the AG-221 45 mg/kg group, which remained on the same dose until study termination at day 130. *P* values for comparisons between treatment groups and vehicle were determined using the log-rank (Mantel–Cox) test. **C,** Percentage of blasts in BM aspirates on last day of treatment (day 84); 200 cells counted per slide from representative mice in each treatment group. Horizontal bars represent the mean; *P* values for comparisons between treatment groups and vehicle were determined using the *t* test. **D,** BM morphology in vehicle, AG-221 45 mg/kg, and Ara-C 2 mg/kg groups. Wright-Giemsa stain, original magnification, ×1,000 oil. Representative results are shown.

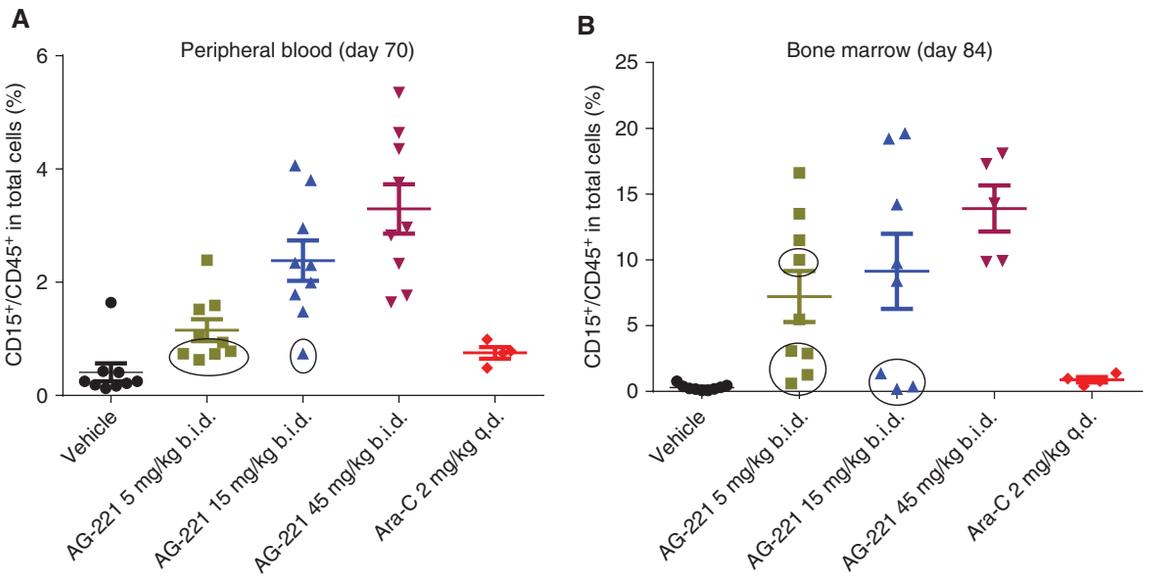

Figure 5. Effects of AG-221 treatment on expression of CD15, a granulocytic marker of differentiation. Percentage of $CD15^+/CD45^+$ cells in the PB (**A**) and BM (**B**) of mice treated with vehicle, AG-221, or low-dose Ara-C, shown as mean ± SEM. Circles indicate mice that died of leukemic disease. q.d., once daily.

TF-1 cell line support a lack of apoptosis induction by AG-221. In contrast to standard chemotherapy, the efficacy of AG-221 therefore appears to derive from induction of differentiation in malignant blasts. This mode of action results in an increase in myeloid differentiation, and production of mature, functional neutrophils, which may be advantageous to patients by avoiding the adverse effects of cytotoxic therapy (e.g., BM aplasia, susceptibility to severe infections, bleeding). In the aggressive AML xenograft mouse model, no changes in the variant allele frequency for other AML-related mutations were observed during AG-221 treatment; however, other patient-derived xenograft models may be suitable for monitoring possible differences in sensitivity of AML subclones to AG-221. Although our models focus on $IDH2^{R140Q}$, *in vitro* studies indicated that AG-221 inhibits 2HG production by the $IDH2^{WT/R172K}$ heterodimer, and *ex vivo* studies demonstrated reduction in intracellular 2HG production and increase in expression of differentiation markers in primary human $IDH2^{R172K}$-mutant AML patient samples, suggesting that AG-221 may also be effective against R172K-mutant tumors. Testing of primary *in vivo* AML models in addition to the four reported was not feasible in this study, owing to the difficulty in engrafting human IDH-mutant leukemia into mice.

The use of differentiation therapy in hematologic malignancies is exemplified by all-trans retinoic acid (ATRA) in acute promyelocytic leukemia (AML subtype M3), which induces blast proliferation followed by terminal differentiation and can induce short-term remission in approximately 85% of patients (40). Combination of ATRA with arsenic trioxide led to much-improved response rates, disease-free survival, and overall survival (40), highlighting the potential utility and synergy of combining differentiation therapy such as AG-221 with traditional chemotherapy or agents with other mechanisms of action, for the treatment of IDH-mutant tumors.

Preliminary data from a phase I trial indicated that AG-221 was well tolerated and had clinical activity in patients with relapsed/refractory AML, MDS, or untreated AML who declined conventional chemotherapy (41). These early results are promising and continue to validate mutant IDH as a therapeutic target. Further understanding of the role of *IDH* mutations in cancer initiation and progression will develop as the clinical data mature and as research broadens to additional mutant IDH-targeted molecules.

METHODS

High-Throughput Screening

Because the $IDH2^{R140Q}$ mutation confers a dramatic increase in affinity for NADPH (Km = 200 nmol/L; Supplementary Fig. S10A and S10B) relative to $IDH2^{WT}$, we configured the screening assay at 10-fold concentration of Km for NADPH and at concentration of Km for αKG, to increase the likelihood of identifying NADPH-uncompetitive and NADPH-noncompetitive inhibitors.

Potency (IC_{50} values) for lead compounds was assessed for the $IDH2^{R140Q}$-mutant homodimer in the presence of NADPH, as described below for AG-221. Cellular potency of lead compounds for 2HG suppression was carried out in a cell line with ectopically expressed $IDH2^{R140Q}$, based on 2HG levels in the culture medium (as detailed below for AG-221).

Synthesis of AG-221

AG-221 was prepared via a four-step process (Supplementary Fig. S1A), beginning with the condensation of methyl 6-(trifluoromethyl)picolinate with biuret to form the aryl substituted triazinedione ring. Chlorination with phosphorous oxychloride yielded the dichlorotriazine. Displacement of the first chlorine with 4-amino-2-trifluoromethylpyridine generated the monochlorotriazine, which could be further reacted with 1-amino-2-methyl-2-propanol to produce AG-221 *[2-Methyl-1-(4-(6-(trifluoromethyl)-pyridin-2-yl)-6-(2-*

(trifluoromethyl)-pyridin-4-ylamino)-1,3,5-triazin-2-ylamino)propan-2-ol]. Further detail is provided in Supplementary Methods.

Expression and Purification of WT and Mutant IDH Enzymes

Proteins were expressed in bacterial or insect cell systems and purified by affinity chromatography. Details are provided in Supplementary Methods.

Determination of Compound Potency (IC_{50} Values)

AG-221 was prepared as 10 mmol/L stock in dimethyl sulfoxide (DMSO) and diluted to 50× final concentration in DMSO. IDH-mutant enzyme activity in converting αKG to 2HG was measured in an end-point assay of NADPH depletion. In this assay, the remaining cofactor was measured at the end of the reaction period by the addition of a catalytic excess of diaphorase and resazurin to generate a fluorescent signal in proportion to the amount of NADPH remaining. $IDH1^{WT}$ and $IDH2^{WT}$ enzyme activity in converting isocitrate to αKG was measured in a continuous assay directly coupling NADPH production to conversion of resazurin to resorufin by diaphorase. In both cases, resorufin was measured via fluorescence (λ_{ex} = 544 nm, λ_{em} = 590 nm). $IDH^{WT/mutant}$ heterodimers were assayed for both WT and mutant activities. Details are provided in Supplementary Methods.

Cell-Based Assays for Measuring Inhibition of 2HG Production

The U87MG human astrocytoma (#HTB-14, ATCC; purchased 2009; not authenticated) and the TF-1 erythroleukemia (#CRL-2003, ATCC; purchased 2011; not authenticated) cell lines were infected with either pLVX-$IDH2^{R140Q}$ or pLVX-$IDH2^{R172K}$, generated from the pLVX-IRES-Neo lentiviral vector (#632181, Clontech Laboratories, Inc.). TF-1 was verified to be growth factor–dependent in a proliferation assay against TF-1a cells (#CRL-2451, ATCC), a growth factor–independent erythroleukemia cell line derived from TF-1 cells. For both cell lines, characterization was carried out after plasmid infection: protein expression was assessed and 2HG levels were continuously monitored to verify authenticity of these overexpression lines. All transduced cell lines were selected and maintained in 500 μg/mL Geneticin in RPMI medium with 10% FBS and penicillin/streptomycin. The endogenous R172K-mutant HCT-116 cell line (HD104-019, Horizon Discovery Group) was purchased in 2013 (not authenticated), and intracellular 2HG levels were assessed to verify IDH2-mutant status.

In order to test the potency of AG-221, cells expressing either $IDH2^{R140Q}$ or $IDH2^{R172K}$ were plated in 96-well microtiter plates overnight at 37°C in 5% CO_2. Compounds were plated in dose response in two columns to generate a seven-point dose response in duplicate. Doses were usually started at 3 μmol/L with 1:3 or 1:10 dilutions. AG-221 was diluted in DMSO to a final concentration of 0.03% DMSO in media. One row of 10 wells was designated for the 0.03% DMSO control. Cells were incubated with compound for 48 hours. Media were removed and 2HG was extracted using 80% aqueous methanol, as previously described, and the measurement of 2HG was expressed as ng/mL in medium (the lower limit of quantification was 10 ng/mL and the upper limit of quantification was 30,000 ng/mL). The data were normalized to the DMSO controls to express percent 2HG suppression as follows: (DMSO 2HG – inhibitor 2HG)/(DMSO 2HG). The percent inhibition values were then plotted against the log of the dose. A sigmoidal dose-response equation using a variable slope was then applied to the data using the following GraphPad equation: log (inhibitor) versus response–variable slope (four parameters). The data were expressed as IC_{50} for 2HG suppression (17).

Protein Purification for X-ray Crystallography Studies

His-tagged protein for cocrystallization of AG-221 was expressed in Sf9 insect cells (#CRL-1711, ATCC) and purified via immobilized metal affinity chromatography, then DEAE and size-exclusion chromatography. Protein for cocrystallization with αKG was expressed in *E. coli* and purified as above. Details are provided in Supplementary Methods.

Crystallization, Data Collection, and Structure Determination

AG-221 co-complex crystals were generated by incubating $IDH2^{R140Q}$ purified from insect cells at 15 mg/mL with 10 mmol/L NADPH and 2 mmol/L of AG-221 or αKG at 4°C for 1 hour. Cocrystals of the complex were grown by hanging drop vapor diffusion technique (HDVD) equilibrating the above mixture with a reservoir solution containing 0.1 mol/L Tris-HCl, pH 8.5, 0.25 mol/L $CaCl_2$, and 25% PEG4000 in a 2:1 ratio at 18°C. For the αKG complex, $IDH2^{R140Q}$ purified from *E. coli* at 15 mg/mL was incubated with 5 mmol/L NADPH, 50 mmol/L of αKG, and 5 mmol/L $CaCl_2$ at 4°C overnight. Co-complex crystals were grown by HDVD equilibrating the mixture with a reservoir solution containing 200 mmol/L magnesium acetate, 100 mmol/L sodium cacodylate, pH 6.5, and 20% PEG8000 in a 1:1 ratio at 18°C.

Crystals were flash-frozen in liquid nitrogen before data collection after equilibrating them in a buffer containing reservoir solution and 20% (v/v) glycerol as a cryoprotectant.

X-ray characterization and data collection for both co-complexes were performed at the Shanghai Synchrotron Radiation Facility. Diffraction data were processed using *HKL2000* (HKL Research Inc.; ref. 42). Crystals were characterized to be of orthorhombic form with space grouping of either $C222_1$ or $P2_12_12_1$. Statistics of data collection, processing, and refinement are summarized in Supplementary Table S7. The structure was determined by molecular replacement with *Phaser* (43) using the structure of IDH2 (Protein Data Bank ID: 4JA8) as a search model. Iterative manual model building and refinement were carried out using *COOT* (44) and *Refmac5* (45) from the *CCP4* package. Examination of difference Fourier map (Fo–Fc) calculations clearly indicated the presence of bound ligands. The electron density maps, contoured around the bound ligands, are shown in Supplementary Fig. S11A and S11B. Two alternative poses were fit for the AG-221 molecule, with the occupancy for each pose modeled at 0.6 and 0.4 in Chains A and B, respectively. Consistent with the ligand binding mode, multiple residues in the binding pocket surrounding AG-221 were also modeled to fit alternative conformations. The final R_{work}/R_{free} for $IDH2^{R140Q}$·AG-221 and $IDH2^{R140Q}$·αKG structures are 0.153/0.194 and 0.142/0.174, respectively. Structure figures were generated using *MOE* (Chemical Computing Group, Inc.) and *PyMOL* (Schroedinger, LLC). Atomic coordinates and experimental structure factors have been deposited at the RCSB Protein Data Bank with accession codes 5I95 for the $IDH2^{R140Q}$·αKG and 5I96 for the $IDH2^{R140Q}$·AG-221 complex structures.

TF-1 Cell Experiments

TF-1 cell experiments were conducted as previously reported (17).

Human IDH2-Mutant AML Samples

All primary *IDH2*-mutant patient AML samples, except AML-4, were provided by Gustave Roussy (Department of Clinical Hematology), according to Institutional Review Board–approved protocols. Informed consent was obtained from all patients, in accordance with the Declaration of Helsinki. AML diagnosis was morphologically proven according to the French–American–British classification. Immunophenotyping and cytogenetic analyses were done locally. Description of the karyotypes follows the International System for Human Cytogenetic Nomenclature. Samples were obtained from PB and/or BM aspirates from patients with $IDH2^{R140Q}$-mutant AML at diagnosis or at relapse. Mononuclear cells were isolated by Ficoll separation. Mutation status was assessed by performing targeted

sequencing of 60 genes frequently mutated in hematologic malignancies using a MiSeq sequencer (Illumina) and a custom panel primer pool, using methods described previously (46, 47). We selected variations using the following criteria: variant allele frequency >10%, variation not reported as polymorphism in SNP databases.

AML-4 corresponds to a human cell line, AMM7577, which was obtained with informed consent from the BM of a male patient with M5 AML who had relapsed and died at 59 years of age. This cell line has a normal karyotype and carries *IDH2*^{R140Q}, *FLT3*-ITD, *DNMT3A*^{R882H}, *NPM1,* and CEBPA insertion.

The clinical characteristics of these samples are indicated in Supplementary Table S3.

Ex Vivo *Cell Culture*

Nine AML samples [*IDH2*^{R140Q}, n = 3 (AML-3, -5, -6); *IDH2*^{R172K}, n = 3 (AML-7, -8, -9); *IDH2*^{WT}, n = 3 (AML-10, -11, -12)] were used, containing more than 70% blast cells, except AML-7. For the latter, leukemic blasts identified as CD45^{int}/SSC^{lo} cells (cells were stained with antihuman CD45 antibody PE-Cy7–hCD45, clone HI30; BD Biosciences) were sorted using a BD Influx Cell Sorter (BD Biosciences). The clinical characteristics of these samples are indicated in Supplementary Table S3. Leukemic cells were cultured in the presence of AG-221 (0.1, 1, or 5 μmol/L) or DMSO (0.1%, v/v, used as a vehicle control) for up to 12 days in StemSpan culture medium supplemented with 0.5% HyClone FCS, human IL3, IL6, stem cell factor, thrombopoietin, EPO, FMS-like tyrosine kinase 3 ligand, granulocyte-macrophage colony-stimulating factor, and granulocyte-colony stimulating factor (all from PeproTech) to sustain cell survival and proliferation, as reported (17). Cell samples were collected at day 8, and flow cytometry analyses were performed to determine phenotype. Antibodies used were as follows (all 1 μg/mL final concentration): PE-Cy7–CD45 (clone HI30), PE–CD11b (clone ICRF44), APC-Cy7–CD14 (clone MφP9), eFluor450–CD15 (clone HI98), and APC–CD24 (clone ML5; all from BD Pharmingen). Intracellular and extracellular levels of D-2HG were determined as previously described (48).

Phagocytosis Assay

Phagocytosis tests were performed with opsonized latex beads as previously reported (49). Briefly, on day 8 of AG-221 treatment, cells were collected and resuspended in RPMI 1640 medium (Thermo Fisher Scientific) supplemented with 10 mmol/L HEPES and 10% heat-inactivated human serum (Invitrogen) to a final concentration of 10^5 cells/mL. Cell cultures were incubated on ø12 mm coverslips in 24-well plates with ø1 μm fluorescent latex beads (Invitrogen), applied at a ratio of approximately 10 beads/cell. After 10-minute centrifugation at 300 g, cells were incubated for 30 minutes at 37°C to initiate phagocytosis prior to fixation in a paraformaldehyde 4% solution (Sigma-Aldrich). Fixed cells were labeled with a mouse monoclonal α-lactoferrin antibody (2B8; Abcam), and DNA was labeled with 4′,6-diamidino-2-phenylindole (DAPI). Labeled cells were imaged with a TCS SP5 confocal microscope (Leica). Neutrophils were identified on the basis of morphologic characteristics (bilobed or multilobed nuclei), and neutrophils with phagocytic activity, defined as neutrophils containing at least one phagocytized bead, were scored in ten fields of view, on approximately 300 total cells. Schematic representations and statistical analyses were performed with the Prism 7 software (GraphPad Software, Inc.).

Mouse Husbandry

All mouse experiments were approved by and performed in accordance with the guidelines and regulations of the Animal Ethics Committee of the Association for Assessment and Accreditation of Laboratory Animal Care International. AML-1, AML-2, and AML-3 mice were housed under pathogen-free conditions at the animal facility of Gustave Roussy. AML-4 mice were housed under pathogen-free conditions in micro-isolator cages at the animal facilities of Crown Bioscience, Inc.

Pharmacokinetic/Pharmacodynamic Study of AG-221 in the U87MG IDH2^{R140Q} Xenograft Model

AG-221 was suspended in 0.5% methyl cellulose and 0.2% Tween 80 in water and given as a single dose of 25 mg/kg or 50 mg/kg, or as two doses of 25 mg/kg 12 hours apart, to 11-week-old female BALB/c nude mice (BK Laboratory Animal Ltd.) with U87MG IDH2^{R140Q} xenograft tumors. A separate group of mice was dosed with the suspension vehicle. Groups of 4 mice were sacrificed at pre-dose, 0.5, 1, 3, 8, 12, 24, 36, 48, and 72 hours after dose to collect tumor samples and blood for plasma analysis. AG-221 and 2HG levels were analyzed by LC/MS-MS.

Primary IDH2^{R140Q} AML Xenotransplantation and AG-221 Treatment

Clinical characteristics and immunophenotypic features of the patients who provided samples to develop these xenograft models are reported in Supplementary Table S3.

For AML-1, AML-2, and AML-3 samples, unsorted AML mononuclear cells (10^6) were transplanted into adult (8–10 weeks old), female, sublethally irradiated (2 Gy) NOD/SCID IL2Rγ−/− (NSG) mice by intrafemoral injection. NSG mice were maintained in pathogen-free conditions. The presence of hCD45$^+$ cells in BM aspirates and in PB was monitored on a monthly basis by flow cytometry using the PE-Cy 7–hCD45 antibody (clone HI30; BD Biosciences) on a BD LSRII flow cytometer (BD Biosciences). Engrafted recipients, assessed by the presence of ≥16% hCD45$^+$ cells in BM, were randomly selected for treatment with either AG-221 30 mg/kg (n = 5) or vehicle solution (n = 5). Investigators were not blinded to treatment group assignment. AG-221 mesylate powder was resuspended by sonication in 6 mg/mL of vehicle solution composed of 0.5% methylcellulose/0.2% Tween 80 diluted in water. Animals were treated b.i.d. by oral gavage for 38 days.

For the AML-4 sample, a total of 50 female 3- to 4-week-old NOD/SCID mice (Beijing HFK Bioscience Co., Ltd.) were engrafted with 2 million frozen cells per mouse (AMM7577 passage 2). PB samples were collected by retro-orbital bleed weekly for FACS analysis starting from week 3, after cell inoculation. Treatment started when the percentage of hCD45$^+$ cells in PB reached an average of 10% of total white blood cells. Mice were randomly allocated to one of five groups and treated with vehicle once daily continuously (group 1), AG-221 at 5, 15, or 45 mg/kg b.i.d. continuously until death or study end (day 84; groups 2–4), or low-dose Ara-C at 2 mg/kg once daily for 5 days (group 5). This was a nonblinded study. The Ara-C dose of 2 mg/kg was selected based on dosing in previous leukemia xenograft mouse models (50) and preliminary experiments using doses of 2 and 10 mg/kg in this model, in which similar efficacy was observed for both doses. The 5-day dosing schedule was intended to mimic the standard 7+3 regimen used in the treatment of AML. We were unable to treat animals with low-dose Ara-C for longer due to the toxicity of this agent in these mice. Treatment was by oral gavage (at 12-hour intervals for AG-221). At day 84, all surviving mice were terminated except for four animals in the AG-221 45 mg/kg group, which remained on the same dose until study termination at day 130 in order to further assess biology and determine if survival was extended.

FACS Analysis of PB, BM, and Spleen Samples

Blood (50 μL) was collected into EDTA tubes by retro-orbital bleeding. Nine volumes of red blood cell lysing buffer (0.8% ammonium chloride solution; Stemcell Technologies) were added to each tube and incubated on ice for 5 minutes. Samples were centrifuged for 5 minutes at 1,500 rpm at 4°C. The supernatant was discarded and cells resuspended with PBS containing 2% FBS. Multicolor FACS analysis was carried out on PB samples using the following antibodies for

models AML-1, AML-2, and AML-3: PE-Cy7–CD45 (clone HI30; eBioscience SAS), FITC–CD14 (clone MφP9; BD Pharmingen), PE–CD11b (clone ICRF44; BD Pharmingen), eFluor450–CD15 (clone HI98, eBioscience), and APC–CD24 (clone ML5; BD Pharmingen). Percentages of human chimerism in blood are indicated in Supplementary Table S8. At sacrifice, human cells were immunophenotyped as single-cell suspensions from PB, spleen, and BM (mixed from tibias, femurs, pelvic bones, and humerus), after lysis of red blood cells with 0.8% ammonium chloride solution (Stemcell Technologies) using the above-mentioned antibodies as well as PE–CD3 (clone HIT3a; BD Pharmingen), PE-Cy7–CD45 (clone HI30; eBioscience SAS), PE-Cy7–CD34 (clone 4H11; eBioscience), and PE–CD117 (c-Kit, clone 104D2; BD Pharmingen). For model AML-4, the following antibodies were used: CD45 (clone HI30; BioLegend) and CD15 (clone W6D3; BioLegend). Data were collected with the BD LSR II system using FACSDiva software (BD Biosciences) and with the BD FACSCalibur system using CellQuest 6 software (BD Biosciences) and analyzed using FlowJo version 9.3.1 software (Tree Star, Inc.).

Histology

The 4% paraformaldehyde-fixed, paraffin-embedded, 4-μm tissue sections were analyzed by HES staining and by standard immunohistochemistry using the anti-hCD45 antibody (clone 2B11+PD7/26; DakoCytomation) or nonspecific IgG1 (DakoCytomation). Images were taken at 100× and 400× magnification using an Axiophot 1 microscope (Zeiss) coupled to a sensicam 12-Bit cooled imaging camera (PCO AG). Morphologic cytology analyses were performed on BM and blood cells after May-Grünwald-Giemsa staining. Image analysis was performed using Definiens Composer software. Regions to be analyzed were first drawn manually and then refined based on automated pattern recognition to separate them into three classes: tumor ($hCD45^+$ cells), white space, and normal cells. Percentage inhibition was calculated as follows: ratio = (% hCD45-positive area)/(% hCD45-positive area + % normal cell area). % h = (ratio vehicle − ratio AG-221)/ratio veh × 100.

IDH2-*Mutant Allele Frequency*

Determination of *IDH2*-mutant allele frequency was carried out by extracting DNA from primary $IDH2^{R140Q}$ and $IDH2^{R172K}$ AML samples before culture, or cells were cultured in the presence of vehicle or 1 μmol/L AG-221 for 9 days, and used as a template for quantitative SNP assay PCR as described (17). At day 9, differentiated cells were sorted by FACS on a BD Influx Cell Sorter (BD Biosciences) according to the expression of differentiation markers CD24, CD15, and/or CD11b. In *in vivo* experiments, DNA was extracted from unsorted BM or spleen samples from AML-1–, AML-2–, and AML-3–engrafted mice treated with AG-221 for 38 days.

Statistical Analyses

No formal sample-size calculations were performed in the xenograft model treatment studies. For the Kaplan–Meier survival curve, statistical significance was determined by the log-rank (Mantel–Cox) test using the survival package in CRAN.

Data Deposition Statement

Atomic coordinates and experimental structure factors have been deposited at the RCSB Protein Data Bank with accession codes 5I95 for the $IDH2^{R140Q}$-αKG and 5I96 for the $IDH2^{R140Q}$-AG-221 complex structures.

Disclosure of Potential Conflicts of Interest

J. Travins has ownership interest (including patents) in Agios Pharmaceuticals. K. Straley has ownership interest in Agios stock. S. Gross has ownership interest (including patents) in Agios Pharmaceuticals. F.G. Salituro has ownership interest in Agios stock and patent applications. S.A. Biller has ownership interest (including patents) in Agios Pharmaceuticals. S.-S.M. Su has ownership interest (including patents) in Agios Pharmaceuticals. No potential conflicts of interest were disclosed by the other authors.

Authors' Contributions

Conception and design: K. Yen, J. Travins, F. Wang, M.D. David, E. Artin, K. Straley, S. Gross, E. Tobin, R. Nagaraja, Z. Konteatis, G. Cianchetta, J.O. Saunders, F.G. Salituro, C. Quivoron, S. de Botton, S. Jin, L. Silverman, H. Yang, L. Dang, V. Penard-Lacronique, S.A. Biller

Development of methodology: K. Yen, J. Travins, F. Wang, K. Straley, S. Gross, E. Tobin, R. Nagaraja, A. Paci, S. de Botton, Y.X. Xu, S. Jin, H. Yang

Acquisition of data (provided animals, acquired and managed patients, provided facilities, etc.): K. Yen, F. Wang, M.D. David, E. Artin, K. Straley, S. Gross, B. DeLaBarre, Y. Chen, R. Nagaraja, C. Quivoron, P. Opolon, V. Saada, S. Broutin, S. de Botton, B.S. Marteyn, F. Jiang, H. Yang, V. Penard-Lacronique

Analysis and interpretation of data (e.g., statistical analysis, biostatistics, computational analysis): K. Yen, F. Wang, M.D. David, E. Artin, K. Straley, A. Padyana, S. Gross, B. DeLaBarre, E. Tobin, R. Nagaraja, S. Choe, L. Jin, Z. Konteatis, G. Cianchetta, C. Quivoron, A. Paci, S. Broutin, S. de Botton, M. Pilichowska, F. Jiang, W. Wei, W. Liu, H. Yang, V. Penard-Lacronique, S.-S.M. Su

Writing, review, and/or revision of the manuscript: K. Yen, J. Travins, F. Wang, M.D. David, E. Artin, K. Straley, A. Padyana, S. Gross, R. Nagaraja, L. Jin, G. Cianchetta, F.G. Salituro, C. Quivoron, S. Broutin, M. Pilichowska, S. Jin, W. Liu, M. Dorsch, V. Penard-Lacronique, S.A. Biller

Administrative, technical, or material support (i.e., reporting or organizing data, constructing databases): K. Yen, F. Wang, J.O. Saunders, O. Bawa, V. Saada, S. Jin

Study supervision: K. Yen, F. Wang, R. Nagaraja, O.A. Bernard, V. Penard-Lacronique, S.A. Biller

Other (image submission): P. Opolon

Other (produced the protein to support assay development): C. Fang

Other (designed research program): S.-S.M. Su

Acknowledgments

This work has benefited from the facilities and expertise of the Imaging and Cytometry Platform (Philippe Rameau), UMS AMMICa, Gustave Roussy Cancer Campus, Villejuif, France. The authors also thank Jean-Baptiste Micol and Christophe Willekens for clinical specimens; Nathalie Auger for cytogenetic analyses; Melanie Polrot (Preclinical Evaluation Platform, Gustave Roussy) for technical assistance with NSG mice; Nicolas Signolle and Marine Bernard (Group of Development in Pathology, SIRIC SOCRATE, grant INCa-DGOS-INSERM 6043) for their expert help with histology analyses; Nathalie Droin for patient sample genotyping; Lionel Mercier for intracellular 2HG measurement; Bing Zhang for help with structure refinement; and Annie Xiaoyu An and Henry Qixiang Li of Crown Bioscience for help with the AMM7577 human AML xenograft mouse model. Writing assistance was provided by Helen Varley, PhD, CMPP, of Excel Scientific Solutions, Horsham, UK, and funded by Agios Pharmaceuticals, Inc.

Grant Support

This work was funded by Agios Pharmaceuticals, Inc., the French National Institute of Health (INSERM-AVIESAN), the National Cancer Institute (INCa-DGOS-Inserm_6043 and INCa 2012-1-RT-09), and the Fondation Association pour la Recherche sur le Cancer (ARC, SL220130607089 Programme Labellisé to V. Penard-Lacronique and S. de Botton). M.D. David is funded by a fellowship from the Institut National du Cancer (INCa-DGOS_5733).

Received September 15, 2016; revised February 8, 2017; accepted February 9, 2017; published OnlineFirst February 13, 2017.

REFERENCES

1. Pavlova NN, Thompson CB. The emerging hallmarks of cancer metabolism. Cell Metab 2016;23:27–47.
2. Hanahan D, Weinberg RA. Hallmarks of cancer: The next generation. Cell 2011;144:646–74.
3. Parsons DW, Jones S, Zhang X, Lin JC, Leary RJ, Angenendt P, et al. An integrated genomic analysis of human glioblastoma multiforme. Science 2008;321:1807–12.
4. Yan H, Parsons DW, Jin G, McLendon R, Rasheed BA, Yuan W, et al. *IDH1* and *IDH2* mutations in gliomas. N Engl J Med 2009;360: 765–73.
5. Mardis ER, Ding L, Dooling DJ, Larson DE, McLellan MD, Chen K, et al. Recurring mutations found by sequencing an acute myeloid leukemia genome. N Engl J Med 2009;361:1058–66.
6. Kosmider O, Gelsi-Boyer V, Slama L, Dreyfus F, Beyne-Rauzy O, Quesnel B, et al. Mutations of *IDH1* and *IDH2* genes in early and accelerated phases of myelodysplastic syndromes and MDS/myeloproliferative neoplasms. Leukemia 2010;24:1094–6.
7. Borger DR, Tanabe KK, Fan KC, Lopez HU, Fantin VR, Straley KS, et al. Frequent mutation of isocitrate dehydrogenase (*IDH)1* and *IDH2* in cholangiocarcinoma identified through broad-based tumor genotyping. Oncologist 2012;17:72–9.
8. Amary MF, Bacsi K, Maggiani F, Damato S, Halai D, Berisha F, et al. *IDH1* and *IDH2* mutations are frequent events in central chondrosarcoma and central and periosteal chondromas but not in other mesenchymal tumours. J Pathol 2011;224:334–43.
9. Gross S, Cairns RA, Minden MD, Driggers EM, Bittinger MA, Jang HG, et al. Cancer-associated metabolite 2-hydroxyglutarate accumulates in acute myelogenous leukemia with isocitrate dehydrogenase 1 and 2 mutations. J Exp Med 2010;207:339–44.
10. Dang L, White DW, Gross S, Bennett BD, Bittinger MA, Driggers EM, et al. Cancer-associated IDH1 mutations produce 2-hydroxyglutarate. Nature 2009;462:739–44.
11. Ward PS, Patel J, Wise DR, Abdel-Wahab O, Bennett BD, Coller HA, et al. The common feature of leukemia-associated IDH1 and IDH2 mutations is a neomorphic enzyme activity converting alpha-ketoglutarate to 2-hydroxyglutarate. Cancer Cell 2010;17:225–34.
12. Chowdhury R, Yeoh KK, Tian YM, Hillringhaus L, Bagg EA, Rose NR, et al. The oncometabolite 2-hydroxyglutarate inhibits histone lysine demethylases. EMBO Rep 2011;12:463–9.
13. Koivunen P, Lee S, Duncan CG, Lopez G, Lu G, Ramkissoon S, et al. Transformation by the (*R*)-enantiomer of 2-hydroxyglutarate linked to EGLN activation. Nature 2012;483:484–8.
14. Xu W, Yang H, Liu Y, Yang Y, Wang P, Kim SH, et al. Oncometabolite 2-hydroxyglutarate is a competitive inhibitor of α-ketoglutarate-dependent dioxygenases. Cancer Cell 2011;19:17–30.
15. Losman JA, Looper RE, Koivunen P, Lee S, Schneider RK, McMahon C, et al. (*R*)-2-hydroxyglutarate is sufficient to promote leukemogenesis and its effects are reversible. Science 2013;339:1621–5.
16. Figueroa ME, Abdel-Wahab O, Lu C, Ward PS, Patel J, Shih A, et al. Leukemic IDH1 and IDH2 mutations result in a hypermethylation phenotype, disrupt TET2 function, and impair hematopoietic differentiation. Cancer Cell 2010;18:553–67.
17. Wang F, Travins J, DeLaBarre B, Penard-Lacronique V, Schalm S, Hansen E, et al. Targeted inhibition of mutant IDH2 in leukemia cells induces cellular differentiation. Science 2013;340:622–6.
18. Turcan S, Rohle D, Goenka A, Walsh LA, Fang F, Yilmaz E, et al. IDH1 mutation is sufficient to establish the glioma hypermethylator phenotype. Nature 2012;483:479–83.
19. Lu C, Ward PS, Kapoor GS, Rohle D, Turcan S, Abdel-Wahab O, et al. IDH mutation impairs histone demethylation and results in a block to cell differentiation. Nature 2012;483:474–8.
20. Saha SK, Parachoniak CA, Ghanta KS, Fitamant J, Ross KN, Najem MS, et al. Mutant IDH inhibits HNF-4α to block hepatocyte differentiation and promote biliary cancer. Nature 2014;513:110–4.
21. Lu C, Venneti S, Akalin A, Fang F, Ward PS, Dematteo RG, et al. Induction of sarcomas by mutant IDH2. Genes Dev 2013;27:1986–98.
22. Okoye-Okafor UC, Bartholdy B, Cartier J, Gao EN, Pietrak B, Rendina AR, et al. New IDH1 mutant inhibitors for treatment of acute myeloid leukemia. Nat Chem Biol 2015;11:878–86.
23. Chen C, Liu Y, Lu C, Cross JR, Morris 4th JP, Shroff AS, et al. Cancer-associated IDH2 mutants drive an acute myeloid leukemia that is susceptible to Brd4 inhibition. Genes Dev 2013;27:1974–85.
24. Kats LM, Reschke M, Taulli R, Pozdnyakova O, Burgess K, Bhargava P, et al. Proto-oncogenic role of mutant *IDH2* in leukemia initiation and maintenance. Cell Stem Cell 2014;14:329–41.
25. Sasaki M, Knobbe CB, Munger JC, Lind EF, Brenner D, Brustle A, et al. IDH1(R132H) mutation increases murine haematopoietic progenitors and alters epigenetics. Nature 2012;488:656–9.
26. Shlush LI, Zandi S, Mitchell A, Chen WC, Brandwein JM, Gupta V, et al. Identification of pre-leukaemic haematopoietic stem cells in acute leukaemia. Nature 2014;506:328–33.
27. Corces-Zimmerman MR, Hong WJ, Weissman IL, Medeiros BC, Majeti R. Preleukemic mutations in human acute myeloid leukemia affect epigenetic regulators and persist in remission. Proc Natl Acad Sci U S A 2014;111:2548–53.
28. Sykes SM, Kokkaliaris KD, Milsom MD, Levine RL, Majeti R. Clonal evolution of preleukemic hematopoietic stem cells in acute myeloid leukemia. Exp Hematol 2015;43:989–92.
29. Marcucci G, Maharry K, Wu YZ, Radmacher MD, Mrozek K, Margeson D, et al. *IDH1* and *IDH2* gene mutations identify novel molecular subsets within de novo cytogenetically normal acute myeloid leukemia: A Cancer and Leukemia Group B study. J Clin Oncol 2010;28:2348–55.
30. Green CL, Evans CM, Zhao L, Hills RK, Burnett AK, Linch DC, et al. The prognostic significance of *IDH2* mutations in AML depends on the location of the mutation. Blood 2011;118:409–12.
31. Losman JA, Kaelin WG Jr. What a difference a hydroxyl makes: Mutant IDH, (*R*)-2-hydroxyglutarate, and cancer. Genes Dev 2013;27: 836–52.
32. Pietrak B, Zhao H, Qi H, Quinn C, Gao E, Boyer JG, et al. A tale of two subunits: How the neomorphic R132H IDH1 mutation enhances production of αHG. Biochemistry 2011;50:4804–12.
33. Yang B, Zhong C, Peng Y, Lai Z, Ding J. Molecular mechanisms of "off-on switch" of activities of human IDH1 by tumor-associated mutation R132H. Cell Res 2010;20:1188–200.
34. Fathi AT, Sadrzadeh H, Borger DR, Ballen KK, Amrein PC, Attar EC, et al. Prospective serial evaluation of 2-hydroxyglutarate, during treatment of newly diagnosed acute myeloid leukemia, to assess disease activity and therapeutic response. Blood 2012;120:4649–52.
35. Cowland JB, Borregaard N. Granulopoiesis and granules of human neutrophils. Immunol Rev 2016;273:11–28.
36. Döhner H, Estey EH, Amadori S, Appelbaum FR, Buchner T, Burnett AK, et al. Diagnosis and management of acute myeloid leukemia in adults: Recommendations from an international expert panel, on behalf of the European LeukemiaNet. Blood 2010;115:453–74.
37. DiNardo CD, Ravandi F, Agresta S, Konopleva M, Takahashi K, Kadia T, et al. Characteristics, clinical outcome and prognostic significance of IDH mutations in AML. Am J Hematol 2015;90:732–6.
38. DiNardo CD, Jabbour E, Ravandi F, Takahashi K, Daver N, Routbort M, et al. IDH1 and IDH2 mutations in myelodysplastic syndromes and role in disease progression. Leukemia 2015;30:980–4.
39. Kernytsky A, Wang F, Hansen E, Schalm S, Straley K, Gliser C, et al. IDH2 mutation-induced histone and DNA hypermethylation is progressively reversed by small-molecule inhibition. Blood 2015;125:296–303.
40. Wang ZY, Chen Z. Acute promyelocytic leukemia: From highly fatal to highly curable. Blood 2008;111:2505–15.
41. Stein EM, DiNardo C, Altman JK, Collins R, DeAngelo DJ, Kantarjian HM, et al. Safety and efficacy of AG-221, a potent inhibitor of mutant IDH2 that promotes differentiation of myeloid cells in patients with advanced hematologic malignancies: Results of a phase 1/2 trial. Blood 2015;126:323.
42. Otwinowski Z, Minor W. Processing of X-ray diffraction data collected in oscillation mode. Methods Enzymol 1997;276:307–26.

43. McCoy AJ, Grosse-Kunstleve RW, Adams PD, Winn MD, Storoni LC, Read RJ. Phaser crystallographic software. J Appl Crystallogr 2007;40:658–74.
44. Emsley P, Lohkamp B, Scott WG, Cowtan K. Features and development of Coot. Acta Crystallogr D Biol Crystallogr 2010;66:486–501.
45. Murshudov GN, Skubak P, Lebedev AA, Pannu NS, Steiner RA, Nicholls RA, et al. *REFMAC5* for the refinement of macromolecular crystal structures. Acta Crystallogr D Biol Crystallogr 2011;D67:355–67.
46. Boissel N, Nibourel O, Renneville A, Gardin C, Reman O, Contentin N, et al. Prognostic impact of isocitrate dehydrogenase enzyme isoforms 1 and 2 mutations in acute myeloid leukemia: A study by the Acute Leukemia French Association group. J Clin Oncol 2010;28:3717–23.
47. Merlevede J, Droin N, Qin T, Meldi K, Yoshida K, Morabito M, et al. Mutation allele burden remains unchanged in chronic myelomonocytic leukaemia responding to hypomethylating agents. Nat Commun 2016;7:10767.
48. Poinsignon V, Mercier L, Nakabayashi K, David MD, Lalli A, Penard-Lacronique V, et al. Quantitation of isocitrate dehydrogenase (IDH)-induced D and L enantiomers of 2-hydroxyglutaric acid in biological fluids by a fully validated liquid tandem mass spectrometry method, suitable for clinical applications. J Chromatogr B Analyt Technol Biomed Life Sci 2016;1022:290–7.
49. Monceaux V, Chiche-Lapierre C, Chaput C, Witko-Sarsat V, Prevost MC, Taylor CT, et al. Anoxia and glucose supplementation preserve neutrophil viability and function. Blood 2016;128:993–1002.
50. Hu S, Niu H, Inaba H, Orwick S, Rose C, Panetta JC, et al. Activity of the multikinase inhibitor sorafenib in combination with cytarabine in acute myeloid leukemia. J Natl Cancer Inst 2011;103:893–905.